Yukuan Li
Di Li ✉
Dongze Wu
Yiqun Wang
Shaoxun Liu
Tao Wang
Xiaokun Wang

https://doi.org/10.21278/TOF.501071424
ISSN 1333-1124
eISSN 1849-1391

THE TEMPERATURE DEPENDENCY OF THE B-W FAILURE CRITERION OF ADVANCED HIGH-STRENGTH DUAL-PHASE STEEL DP780

Summary

The Bao-Wierzbicki (B-W) criterion more accurately describes the fracture characteristics of steel under different stress states and provides a more precise prediction of the fracture of duplex steels. Taking DP780 as a research object, the relationship between stress triaxiality and fracture strain in the fracture region of dual-phase steel at different temperatures was investigated by uniaxial tensile, shear, and Nakazima tests combined with numerical simulations. A stress triaxiality-based fracture model (B-W fracture criterion) at different temperatures was obtained and its temperature dependence was studied. Finally, the reliability of the criterion was verified using the stretch-bending tests of U-shape parts. The fracture criterion can be employed to forecast the emergence of fractures in automotive components during the stamping processes. This enables designers to undertake virtual simulations of operational conditions, thereby facilitating the selection of optimal process parameters during production.

Key words: *advanced high-strength dual-phase steel; B-W criterion; DP780; stress triaxiality; temperature dependence*

1. Introduction

Advanced high-strength steels have been a pivotal factor in the accelerated evolution of the modern automobile industry. Among these materials, dual-phase steels have gained prominence in automotive structural components and body materials, enabling effective structural weight reduction and enhanced automotive safety. This is attributed to their exemplary mechanical comprehensive performance, favourable welding and painting characteristics, and cost-effectiveness [1]. However, dual-phase steels are prone to fracturing during the stamping process[2], which results in the generation of scrap. This not only significantly impacts the quality of the product but also inflicts irreparable economic losses on

the enterprise. Therefore, it is highly important to establish accurate fracture criteria for metallic materials through a combination of experiments and numerical simulations to predict potential failures [3].

Bao and Wierzbicki [4] conducted a series of material property experiments on 2024 aluminium alloy specimens, including upsetting, shear, and tensile tests. Their findings indicate that the fracture strain does not vary monotonically with stress triaxiality. In response, they proposed a segmented function representation of the B-W fracture criterion to characterise the relationship between the fracture strain and stress triaxiality, as shown in Fig. 1.

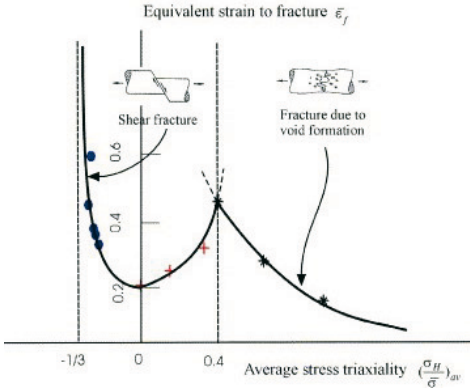

Fig. 1 Dependence of the equivalent strain to fracture on the stress triaxiality

The B-W criterion better describes the fracture characteristics of steel under different stress states, so many scholars in China and abroad have studied the B-W criterion for a variety of materials. Gui [5] analysed the applicability of several commonly used failure criteria to dual-phase steel and found that B-W criteria can better predict the fracture of dual-phase steel. Similarly, Yu [6] conducted a comparative analysis and determined that the B-W criterion was moderately accurate for characterising the fracture behaviour of ductile materials. Yu [7] constructed the variation relationship between the fracture strain and stress triaxiality of 30CrMnSiNi2A steel and determined the parameters of the B-W failure model, which better describes the fracture characteristics of this steel under different stress states. Ying [8] calculated the B-W fracture criterion based on the method of finite element modified mean stress triaxiality values for mild steel specimens under multiple stress states, fitted the B-W fracture criterion, and was able to better predict the fracture behaviour under complex stress states. Guo [9] corrected the failure strain temperature term based on experimental and numerical simulation results and proposed a B-W failure criterion for Q235 steel based on the J-C failure model. Chen [10] used static and dynamic experiments to test the failure strains of TC4 titanium alloy in triaxiality at different stress states and performed segmental fitting to obtain the B-W failure criterion, on the basis of which the fracture failure coefficients of the material were verified by impact experiments and the numerical simulation of the material. Fu [11] established a B-W failure model of DP780 duplex steel at room temperature by combining experiments and numerical simulations. Zhao [12] investigated the influence of stress triaxiality on the fracture strain of 7075 cast aluminium alloy through quasi-static tensile testing, thereby developing a fracture prediction model for the fracture strain and stress triaxiality of 7075 cast aluminium alloy. It has been shown that the B-W criterion exhibits high accuracy in the fracture prediction of dual-phase steel moulding. However, most of the studies have been carried out at room temperature and there are fewer temperature-related criterion studies to predict fracture under warm forming conditions. Accordingly, this study concentrates on the B-W criterion and the temperature dependence of DP780 plates under warm moulding conditions (298 K-873 K), employing the B-W criterion to anticipate fracture under elevated temperatures.

In this study, DP780 dual-phase steel is the focus of investigation where uniaxial tensile, shear, and Nakazima tests are conducted at varying temperatures to obtain the performance data of sheet metal. These data are then integrated with numerical simulations to determine the relationship between the stress triaxiality of each stress state and the fracture strain. This is achieved through the Modified Mohr–Coulomb (MMC) criterion in ABAQUS. The objective of the study is to ascertain the B-W fracture criterion for DP780 within the temperature range of 298 K to 873 K and to examine the correlation between the criterion and the temperature.

2. Experiments

2.1 Material

In this paper, the advanced high-strength dual-phase steel plate DP780 produced by Shanghai Baosteel was utilised as the test material. The thickness of the plate was 1 mm. Its chemical composition is presented in Table 1.

Table 1 Chemical composition of DP780 and its mass fraction%

Steel	C	Si	Mn	P	S	Al
DP780	0.1	0.16	2.02	0.008	0.003	0.039

2.2 Uniaxial Tensile Test

In order to study the thermomechanical properties of DP780 steel, uniaxial tensile tests were carried out on DP780 steel at different temperatures using a WDW-20D material property testing machine (Fig.2) The machine is widely used in metal and non-metal tensile, compression, bending, and other mechanical properties of the test. It has a maximum test force of 20 kN and a speed range of 0.01-500 mm/min. A high-temperature heating furnace was used to heat the specimens, with a temperature control system that can be realised in the range of 100-1100 °C within a temperature precision adjustment. The extensometer is a non-contact electronic extensometer that accurately measures the strain of a material during the tensile process over a range of ± 1%-± 50% [13].

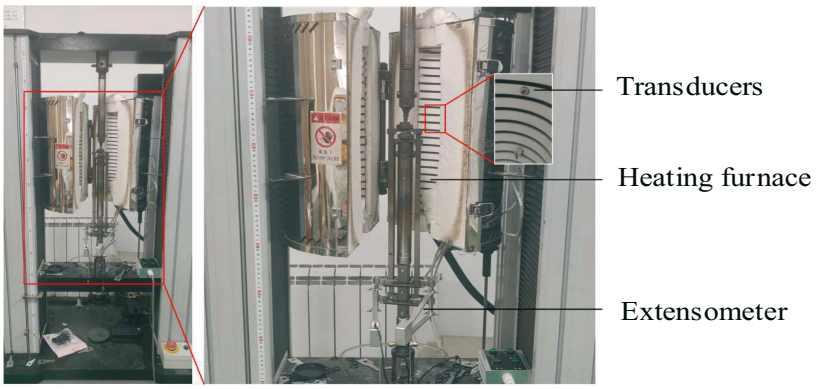

Fig. 2 WDW-20D material property testing machine

The sample size is designed according to the Chinese GB/T4338-2006 [14] standard, as shown in Fig. 3. Laser cutting was used to manufacture samples from the same sheet in the rolling direction.

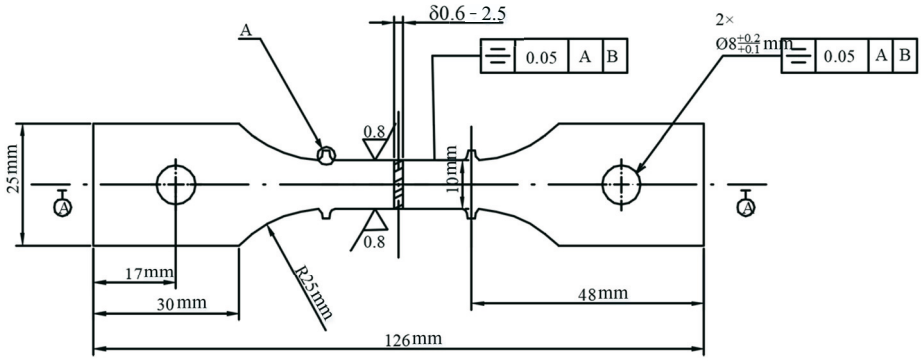

Fig. 3 Dimensions of the specimen

Dual-phase steel plate specimens were subjected to high-temperature uniaxial tensile tests at 298 K, 473 K, 573 K, 673 K, 773 K, and 873 K, respectively. One specimen was used for each temperature, with a strain rate of 1×10^{-4} s^{-1}. The samples after the tensile tests are shown in Fig. 4. Through the test, the relevant material property parameters of the steel plate at different tensile temperatures, such as yield strength, tensile strength, etc., can be obtained directly. The true stress-strain curves obtained after the deformation of DP780 are shown in Fig. 5.

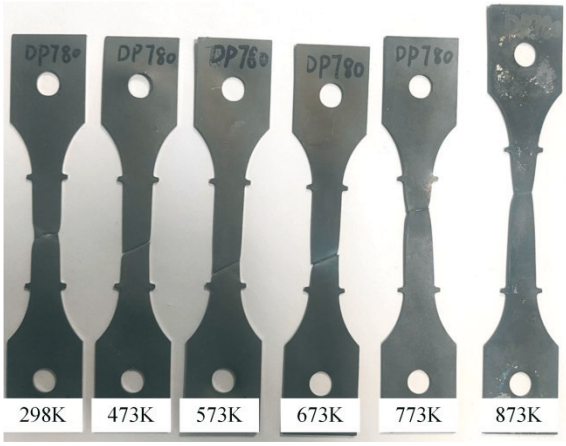

Fig. 4 Unidirectional tensile test results of DP780 steel at different temperatures

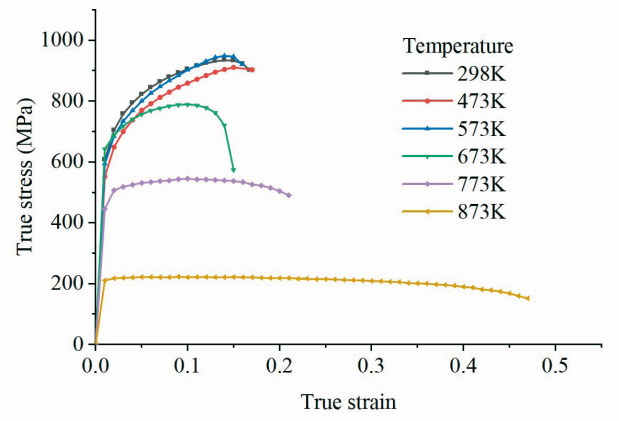

Fig. 5 True stress–strain curves in different temperatures

In this paper, the Swift model was used to fit the stress–strain curve for the uniform extension of its plastic segment, the expression of which is shown in Equation (1). The fitted curves are shown in Fig. 6. The values of K and n at different temperatures are shown in Table 2.

$$\sigma = K(\varepsilon_0 + \varepsilon_p)^n \tag{1}$$

where K is the hardening coefficient, n is the hardening index, ε_0 is the pre-strain, ε_p is the plastic strain, and σ is the stress.

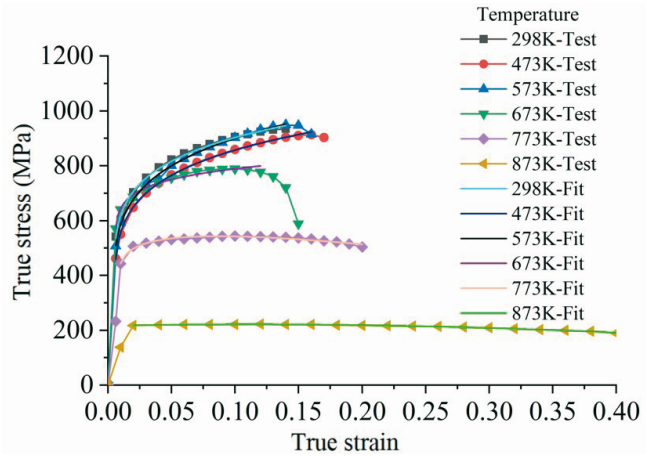

Fig. 6 The fitted curves of the Swift model

Table 2 The K and n of sheet metal at different temperatures

	298 K	473 K	573 K	673 K	773 K	873 K
K	1305	1700	1518	1015	456.6	257.6
n	0.14	0.21	0.16	0.116	0.076	0.069

2.3 Shear test

In order to ascertain the strain and stress state of the plate in disparate shear fracture states, six shear specimens with varying angles were devised in this study, as illustrated in Fig. 7. As the shear angle in the central region of the specimen increases, the stress state in the central region undergoes a transition from pure shear to a mixed tensile-shear state, and subsequently to a pure tensile state.

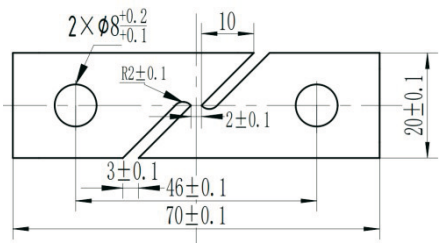

(a) 0°shear specimen

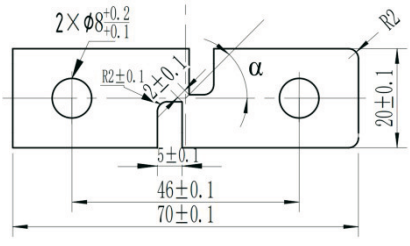

(b) α = 15°,30°,45°,60° shear specimens

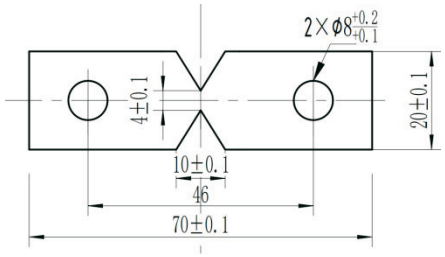

(c) 90°shear specimen

Fig. 7 Dimensions of shear specimens at different angle

The different angle shear specimens were mounted on a tensile testing machine to carry out the corresponding tests at a strain rate of 0.0001 s^{-1}. The temperature of the heating furnace attached to the tensile testing machine was set at 298 K, 473 K, 573 K, 673 K, 773 K, and 873 K. Six different angle tests were conducted at each temperature, for a total of 36 specimens. The fracture specimen at 298K is shown in Fig. 8.

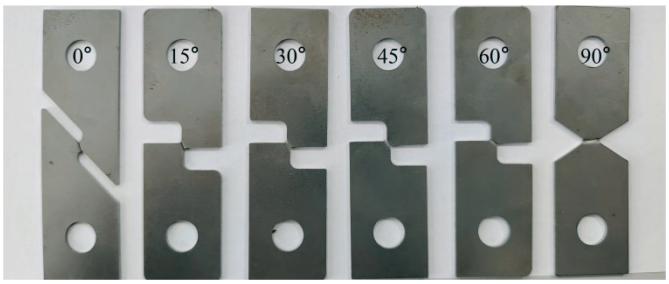

Fig. 8 Shear fracture specimens

The load-displacement curves measured in the tests are shown in Fig. 9. (Among them, 0°, 30°, 60° are published in reference [15]). At the same temperature, the force required to fracture a specimen increases as the angle increases. The reason for this is that the specimen is more susceptible to fracture when it is subjected to shear stress. An increase in the specimen angle results in a reduction in the shear percentage, an increase in the tensile percentage, and a transition from a pure shear stress state to a pure tensile stress state. This enables the material to withstand greater stress.

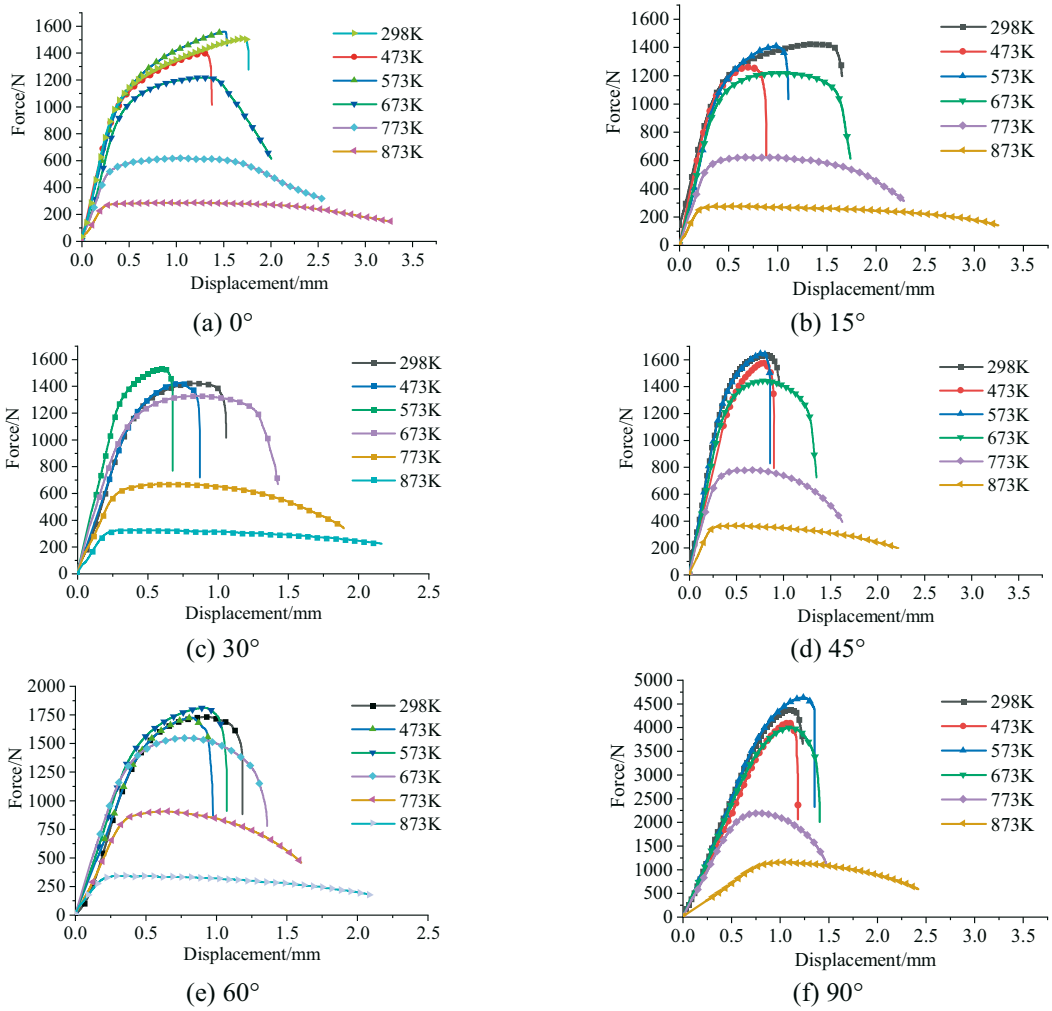

Fig. 9 Load-displacement curves of the shear tests.

2.4 Nakazima test

The forming limits under different stress states were obtained through the Nakazima test on specimens of varying dimensions. The dimensions of the Nakazima test specimen were determined in accordance with the national standard GB/T15825.8-2008 [16]. The specific style and shape are illustrated in Fig. 10, and the design dimensions are presented in Table 3 [17].

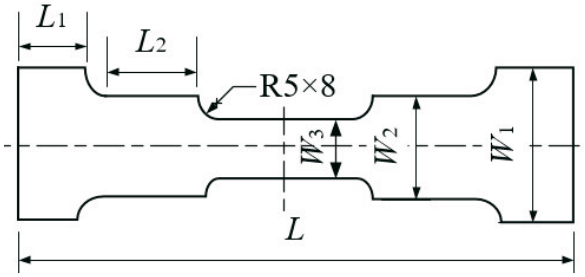

Fig. 10 Dimensions of expanded sheet

Table 3 Dimensions of bulging specimen

Dimensions	Specimens								
	1	2	3	4	5	6	7	8	9
L	180	180	180	180	180	180	180	180	180
L1	40	40	40	40	40	-	-	-	-
L2	20	20	20	20	20	-	-	-	-
W1	40	60	80	100	120	120	120	160	180
W2	30	50	70	90	110	120	140	160	180
W3	20	40	60	80	100	120	140	160	180

The Nakazima test was conducted using a YZ32-160S CNC press machine, which mainly comprises a die, punch (R=50 mm), binder, draw beads, and other components, as shown in Fig. 11.

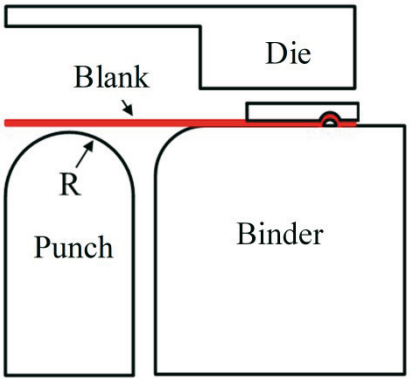

Fig. 11 Mould diagram of the bulging test

Nakazima tests were performed at 298 K, 473 K, 573 K, 673 K, 773 K, and 873 K. Only one test was performed for each size of specimens at each temperature. Prior to the stamping test, the plate specimen should be heated to the corresponding specific temperature in the high-temperature furnace and maintained at that temperature for five minutes. Concurrently, the mould should be heated to the corresponding temperature. Subsequently, the sheet is positioned on a stamping die, and the specimen is initially crimped using a concave die. This is followed by the application of a controlled hydraulic press to eject the convex die. The stamping process is terminated when the specimen shows signs of fracture. The fracture specimen is illustrated in Fig. 12.

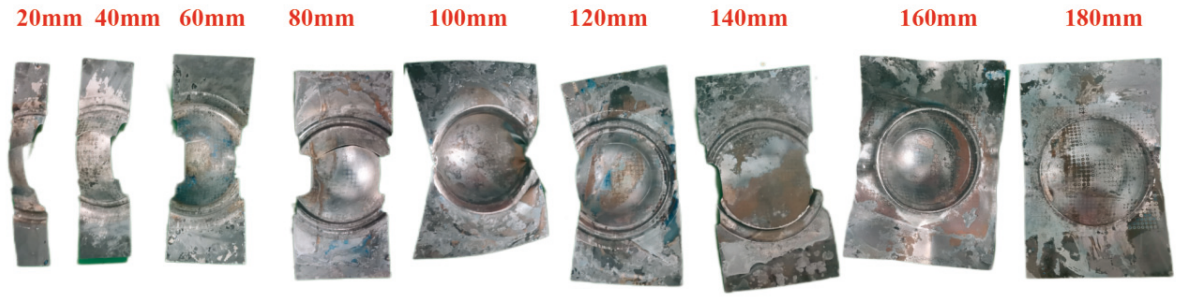

Fig. 12 Nakazima test fracture specimens

Upon examination of the fractured specimens illustrated in Fig.12, it becomes evident that the fracture patterns observed in specimens of varying sizes are largely similar, occurring at approximately the same location. The majority of these fractures manifest near the centre of the specimen, resulting in a curved fracture trajectory.

3. B-W criterion

3.1 MMC criterion

In order to determine the fracture point of dual-phase steel, this paper adopts the MMC criterion as the fracture criterion. Bai and Wierzbicki introduced their research on the generalised hardening criterion [18], which modified the Mohr Coulomb criterion in the field of geotechnical engineering. They also proposed a modified Mohr Coulomb criterion [19], which can better simulate brittle fracture and ductile failure of metallic materials [20]. The expression for the MMC criterion is shown in equation (2):

$$\hat{\varepsilon}_f = \left\{ \frac{K}{c_2} \left[c_3 + \frac{\sqrt{3}}{2-\sqrt{3}} (1-c_3) \left(\sec\left(\frac{\bar{\theta}\pi}{6} \right) - 1 \right) \right] \right.$$
$$\left. \times \left[\sqrt{\frac{1+c_1^2}{3}} \cos\left(\frac{\bar{\theta}\pi}{6} \right) + c_1 \left(\eta + \frac{1}{3} \sin\left(\frac{\bar{\theta}\pi}{6} \right) \right) \right] \right\}^{-\frac{1}{n}} \tag{2}$$

where K is the hardening coefficient, n is the hardening index, c_i is the parameters to be determined, η is the stress triaxiality, and $\bar{\theta}$ is the Lode angle parameter, which is a dimensionless quantity. The lode angle is the angle between the first principal stress and the deviatoric stress component.

The MMC criterion is more widely used to predict the shear fracture damage of dual-phase steels due to its favourable computational stability, the necessity to identify a smaller number of parameters, and the simplicity of identification based on experimental data [21]. The MMC criterion parameters have been calibrated in previous studies [15], so the VUMAT subroutine with the MMC criterion was used in the simulations in this paper to determine the fracture of the steel plate.

3.2 Stress triaxiality

Stress triaxiality is a dimensionless parameter that reflects the state of triaxial stress within the stress field and the degree of constraint on material deformation. Consequently, it directly affects the plastic deformation of the material and the behaviour of breakage [22]. Stress triaxiality is typically expressed in the stress field as the ratio of the hydrostatic stress to the Mises equivalent stress, as illustrated in the following expression:

$$\eta = \frac{\sigma_m}{\sigma_e} = \frac{\frac{\sigma_1 + \sigma_2 + \sigma_3}{3}}{\sqrt{\frac{(\sigma_1 - \sigma_2)^2 + (\sigma_2 - \sigma_3)^2 + (\sigma_1 - \sigma_3)^2}{2}}} \tag{3}$$

where η is the stress triaxiality, σ_m is the hydrostatic stress, σ_e is the equivalent stress, σ_1, σ_2, σ_3 are the principal stresses in the three directions.

For specific materials in a certain range, the stress triaxiality value is high, the stress state is biased towards the tensile state, and the material is more susceptible to tensile fracture. Conversely, when the stress triaxiality value is small, the stress state is biased towards compression, and the material is more prone to shear fracture [23]. In a pure shear condition, the stress triaxiality is zero.

To establish the B-W fracture criterion of DP780, it is necessary to extract the stress triaxiality and equivalent plastic strain at fracture failure under different stress states. As the stress triaxiality cannot be obtained directly from the tests themselves, it is necessary to use a combination of tests and simulations to obtain the stress triaxiality at fracture failure. The MMC criterion was employed as the instability criterion and incorporated into the VUMAT subroutine. The uniaxial tensile, shear and Nakazima tests were simulated using ABAQUS simulation software, and the stress triaxiality and equivalent plastic strain were subsequently extracted. The preliminary B-W curve data points were obtained.

3.3 Shear simulation

In ABAQUS simulation software, simulation models of shear samples at different angles were established according to the sample sizes as shown in Fig. 7. The finite element models of the shear samples at various angles are shown in Fig.13. In order to obtain more accurate simulation data, the grid in the centre region of the specimen was refined, and the size of the centre grid cell was set to 0.4 mm×0.4 mm. Furthermore, to facilitate the expeditious completion of the simulation, the dimensions of the remaining grid cells were set to 1 mm×1 mm. The total number of grids was approximately 2800 [24].

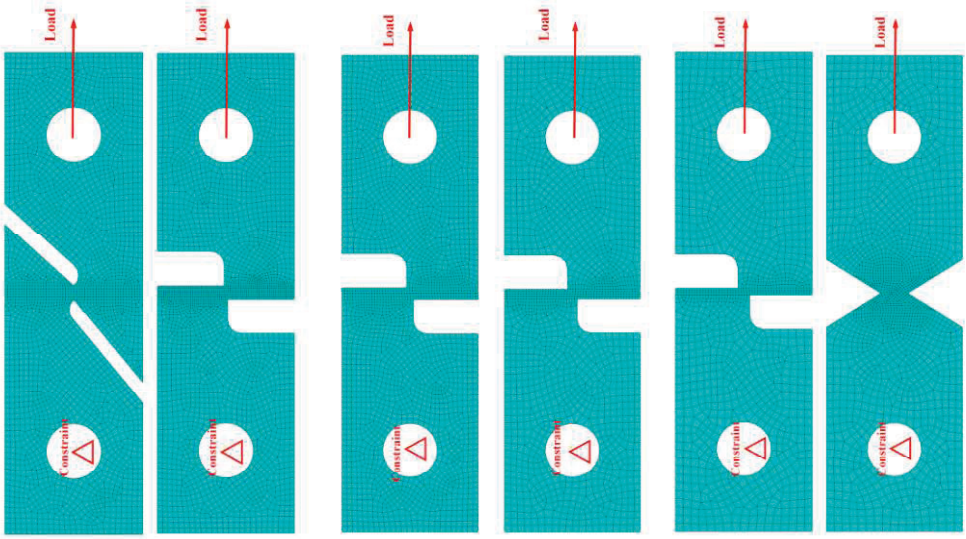

Fig. 13 Finite element model of the specimens at various angles

Once the model had been established, tensile test simulations were conducted. The results of the stress triaxiality simulation at the moment of tensile fracture are shown in Fig. 14.

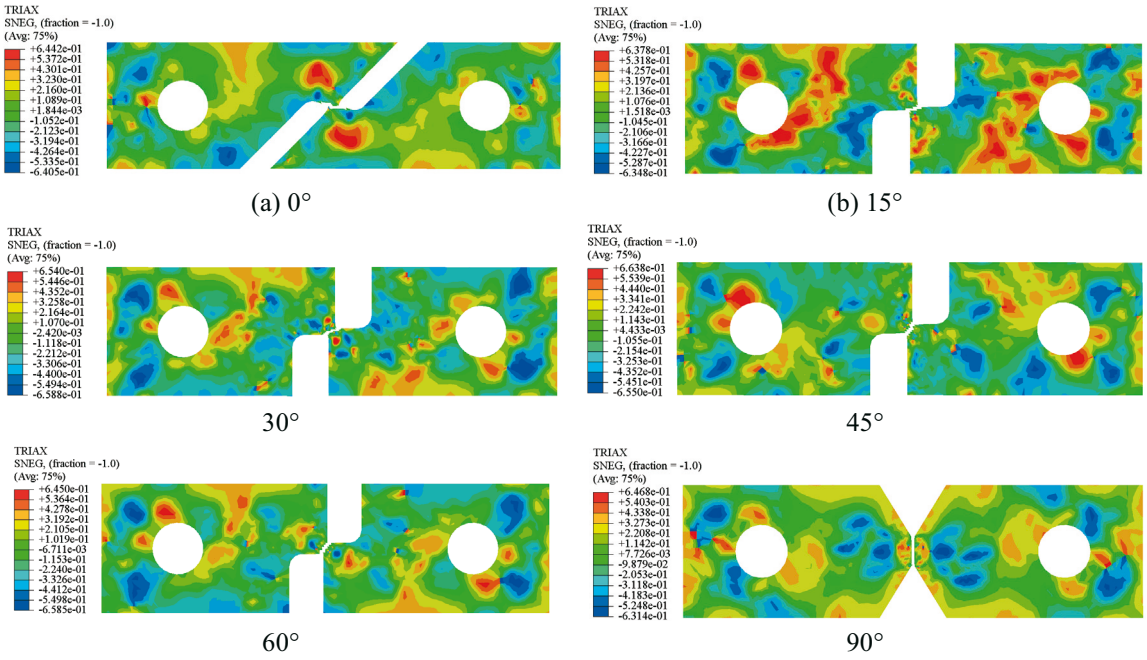

Fig. 14 Results of shear simulation stress triaxiality

The stress triaxiality at the moment preceding fracture was extracted and found to be predominantly between 0 and 0.3, with an increase in the specimen shear angle. This shows that the stress state at the centre of the specimen changes from pure shear to tension shear mixing, and finally to a pure tensile state.

3.4 Uniaxial tensile and Nakazima simulation

A uniaxial tensile sample was modelled in ABAQUS simulation software according to the above sample specifications, as shown in Fig. 15. The total number of specimen model meshes was approximately 3,400.

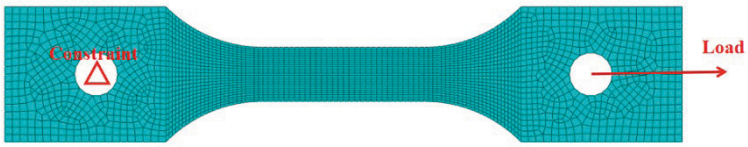

Fig. 15 Finite element modelling of a uniaxial tensile specimen

Once the modelling process was concluded, one end of the specimen was affixed, while the other end was subjected to a tensile strain rate of 1×10^{-4} s^{-1}. The result of the fracture stress triaxiality simulation is presented in Fig. 16. The stress triaxiality and the equivalent plastic strain at the instant preceding the fracture were extracted.

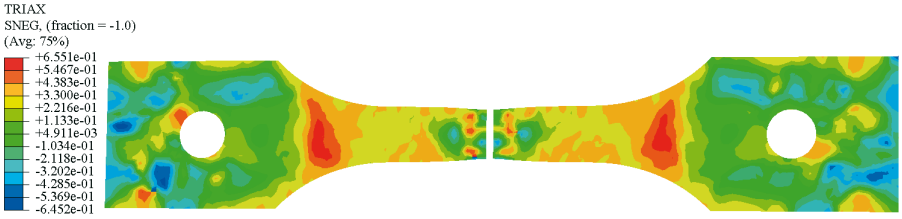

Fig. 16 Results of tensile simulation stress triaxiality

In accordance with the specifications of the YZ32-160SCNC hydraulic press mould, the stamping simulation model was constructed in ABAQUS 6.14-4, as illustrated in Fig. 17.

Given the difficulty of deforming the die, punch, and binder, they were set as rigid bodies to enhance the efficiency of the calculations. A sheet with a grid size of 1 mm×1 mm and a thickness of 1 mm is shown in Fig. 18.

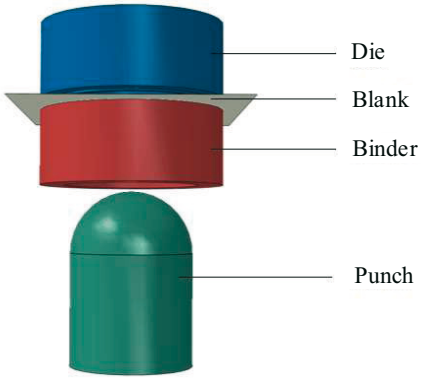

Fig. 17 Nakazima test mould model

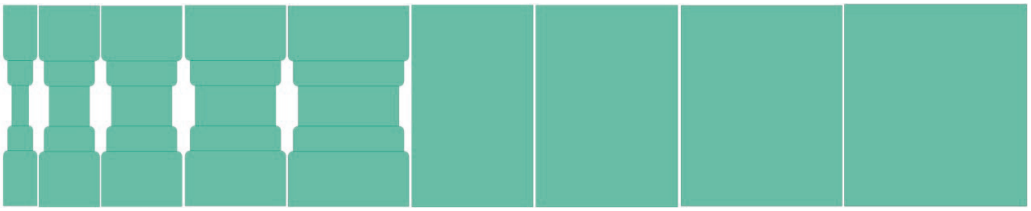

Fig. 18 Sheets of different sizes

During the course of the simulation, the die was lowered to compress the sheet. Thereafter, the punch was ejected upwards, and the simulation was concluded when the sheet broke. The stress triaxiality results of the Nakazima simulation and fracture simulation are presented in Fig. 19.

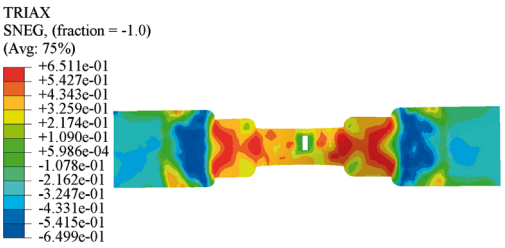

(**a**) W_1= 20 mm

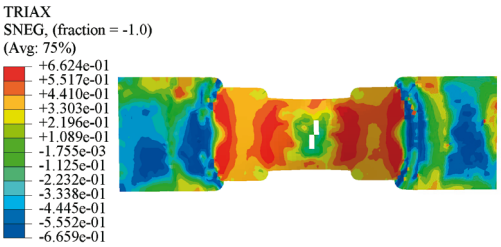

(**b**) W_1= 40 mm

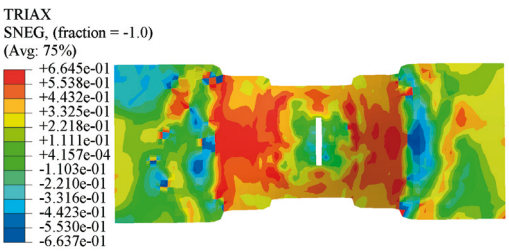

(**c**) W_1= 60 mm

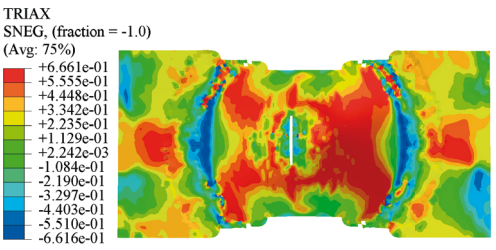

(**d**) W_1= 80 mm

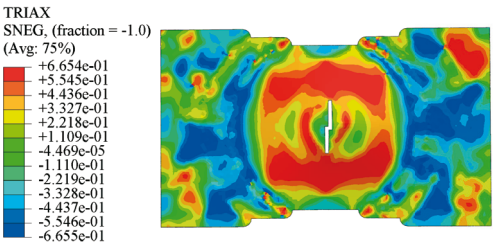

(**e**) W_1= 100 mm

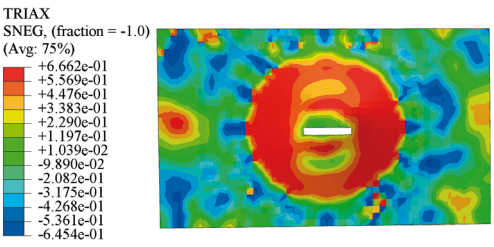

(**f**) W_1= 120 mm

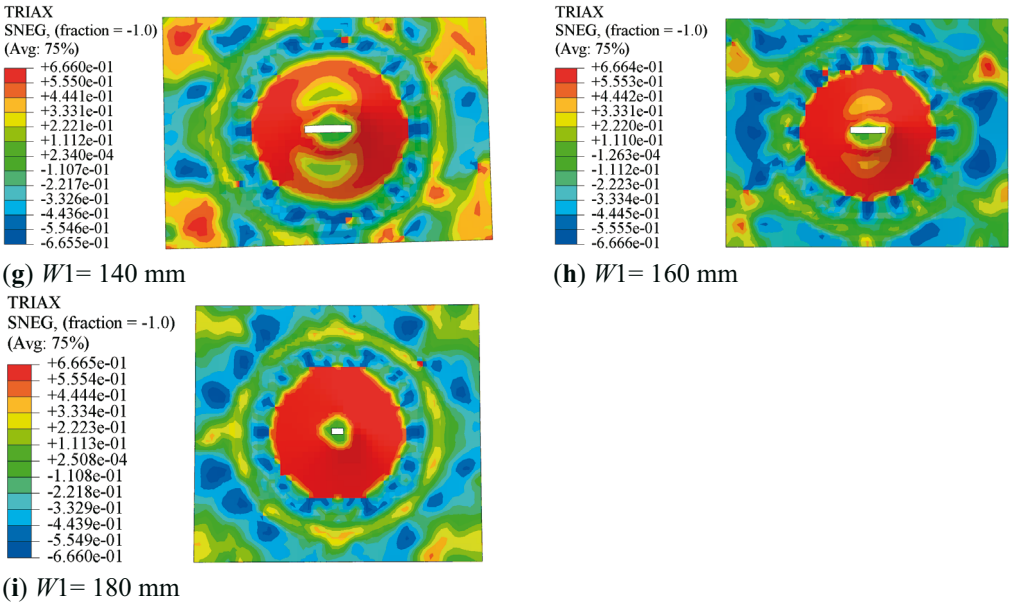

Fig. 19 Results of Nakazima simulation stress triaxiality

Stress triaxiality at the moment preceding the fracture of the uniaxial tensile and Nakazima simulation specimens was extracted and found to be predominantly within the range of 0.3-0.666. This value increased with the expansion of the sheet size, indicating a transition in the stress state at the centre of the specimen, from single-tension to double-tension.

3.5 Establishing the B-W fracture criterion

In the process of metal forming, any stress triaxial degree corresponds to a fracture strain. This series of corresponding stress triaxiality and fracture equivalent strain constitutes a fracture curve, which is the fracture criterion established in this paper [25]. In this section, the stress triaxiality and equivalent plastic strain obtained from uniaxial tensile, shear, and Nakazima simulations at different temperatures are fitted to establish the fracture criterion under DP780 temperature forming. The B-W curves were derived by aggregating the data points for each stress state, as illustrated in Fig. 20. In the metal forming process, when the equivalent strain at a certain place of the material is greater than its critical fracture strain, the failure fracture occurs; otherwise, no failure fracture occurs.

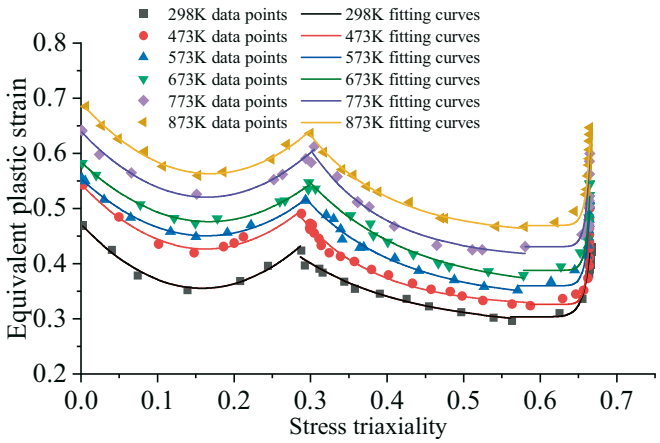

Fig. 20 B-W curves at different temperatures

In the range of stress triaxiality between 0 and 0.3, the equivalent plastic strain exhibits a quadratic curve distribution, displaying a decrease and subsequent increase with the rise in

stress triaxiality. When the stress triaxiality is within the range of 0.3 to 0.6, the equivalent plastic strain declines at a gradual and exponential rate as the stress triaxiality rises. The equivalent plastic strain attains a minimum value near 0.6. This is followed by an exponential increase, which grows sharply around 0.666 and reaches a maximum value.

As the temperature rises, the equivalent plastic strain at fracture also increases. This indicates that the threshold for fracture of the dual-phase steel sheet increases with the rising temperature under warm forming conditions and the forming properties of the sheet are further improved. The expression for the B-W fracture criterion, derived after the introduction of the temperature, is presented in equation (4):

$$\varepsilon_p = \begin{cases} 4.4412\eta^2 - 1.4553\eta + 0.00036375T + 0.3601 & 0 \le \eta < 0.3 \\ 0.16252 + 0.000311176T + 3.05268 \times 0.0000400633^{\eta} & 0.3 \le \eta < 0.6 \\ 2.48422e^{426.8675\eta} + 0.000293828T + 0.20475 & 0.6 \le \eta \end{cases} \quad (4)$$

where ε_p is the equivalent plastic strain, η is the stress triaxiality, and T is the temperature (298K-873K).

4. Validation

The B-W fracture criterion was written into the VUMAT subroutine for a simulation analysis of the U-piece tension-bending tests to verify the accuracy of the resulting fracture failure criterion. The U-piece tension-bending test employed stamping dies with convex fillet radii of 1 mm, 5 mm, and 10 mm to simulate the shear fracture and tension-shear mixed fracture that may occur in actual part processing. The U-piece bending mould is shown in Fig. 21. The U-piece bending specimens were prepared from DP780 dual-phase steel plate material with dimensions of 250 mm in length, 30 mm in width, and 1 mm in thickness.

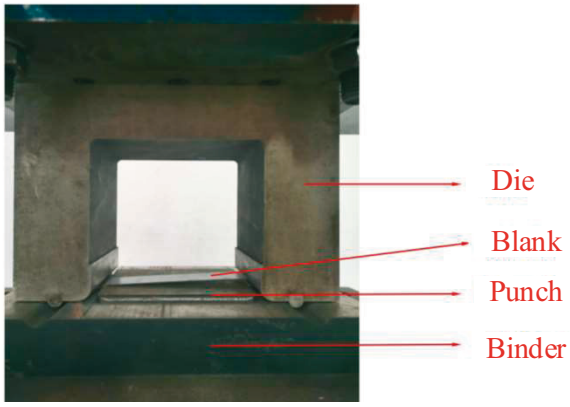

Fig. 21 Specimen stretch-bending die

Before the U-piece bending fracture test, the plate was heated to 723K using a high-temperature furnace and held for 5 min, while the mould was heated to the corresponding temperature. Then, the sheet was quickly placed on the stamping die for stamping, and when the sheet appeared to break, the stamping stopped and the ejection height of the convex die was recorded. The fracture appearance of the specimens at different punch rounding angles are shown in Fig. 22.

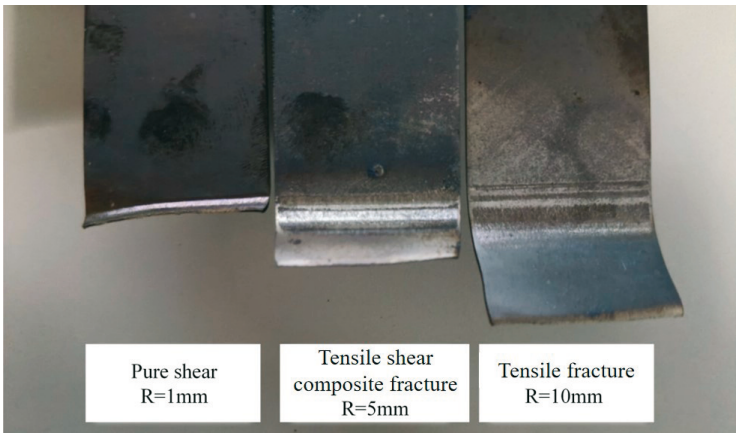

Fig. 22 Specimen fracture position

According to the actual dimensions of the mould and sheets, a finite element simulation model of the U-piece bending specimen was established in ABAQUS, as shown in Fig. 23. The mould was set as a rigid body to improve the efficiency of the model calculation. The sheet unit was designated as a shell unit of S4R, the size of the divided grid cell was 1 mm×1 mm, and the overall number of cells was 3800. The simulation used the VUMAT subroutine containing the B-W fracture criterion.

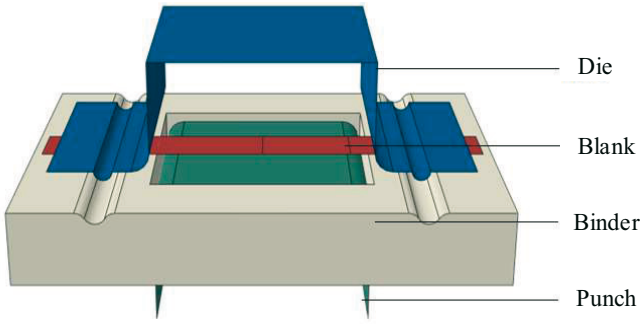

Fig. 23 Stretch-bending mould model

The simulation results of tension bending under different radii of the convex mould are shown in Fig. 24, and the simulated fracture location and fracture morphology are similar to the test results. Table 4 presents a comparative analysis of the sheet simulation and the press depth data at the moment of the sheet fracture during the test. As illustrated in Table 4, the simulation outcomes for the sheet fracture exhibit a lower degree of discrepancy with the experimental data. It can be seen that the B-W fracture failure criterion at each temperature is accurate and enables the accurate prediction of fracture under the warm forming conditions of the sheet.

(**a**)

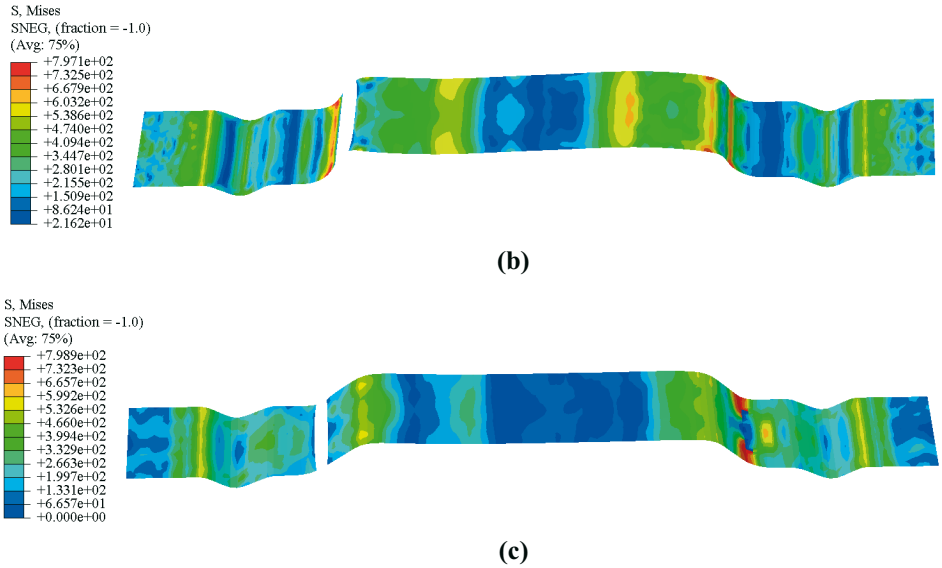

Fig. 24 Simulation of drawing and bending moulding

Table 4 Depth of punch with different fillet radii

Punch Fillet Radius *Rp* /mm	Test Press Depth *d*1 /mm	Simulation of Stamping Depth *d*2 /mm	Error (%)
1	8.4	7.9	5.9
5	10.2	9.5	6.8
10	12.0	11.5	4.9

Meanwhile, the stress triaxiality and equivalent plastic strain at the fracture were obtained by simulation, as shown in Figs. 25 and 26, and combined with the B-W curve to assess the accuracy of the criterion, as shown in Fig. 27.

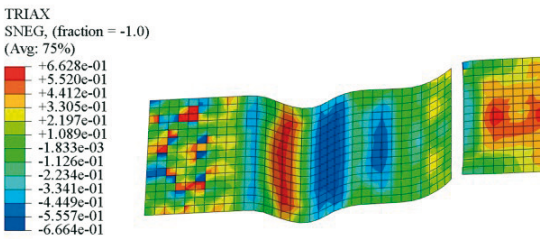

Fig. 25 Triaxial stress nephogram

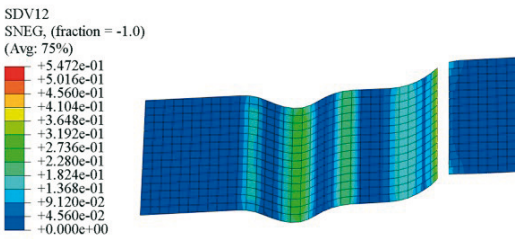

Fig. 26 Equivalent plastic strain nephogram

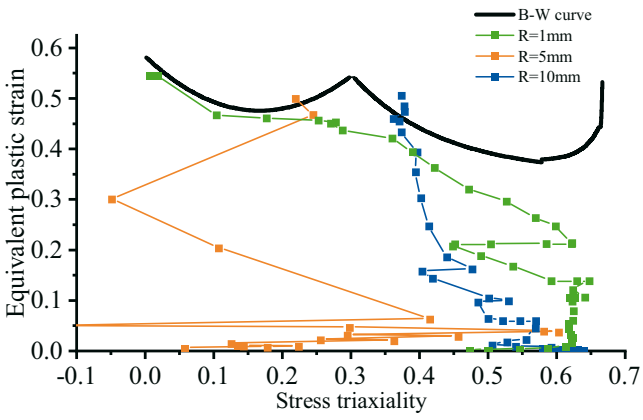

Fig. 27 The criterion curve of B-W

The curves in Fig. 27 show the dynamic trajectories of stress triaxiality and equivalent plastic strain during the bending process. The stress triaxiality and equivalent plastic strain constantly change, and the change trajectory becomes more complex. The final result shows that the unit has been in a failure state, which is consistent with the results of the test where the fracture occurs. This indicates that the B-W curve established in this paper is effective as a criterion for predicting the fracture of two-phase steel.

5. Conclusions

In this study, a combination of experimental and numerical techniques was employed to ascertain a stress triaxiality-based fracture criterion (B-W criterion) for DP780 sheet at varying temperatures. The relationship between stress triaxiality and equivalent plastic strain at the moment of fracture of DP780 sheet was obtained by studying specimens in different stress states. Furthermore, a unified expression of the B-W criterion, which considers the effect of temperature, was established by incorporating temperature into the B-W fracture criterion.

1. Initially, tests and simulations were conducted on shear specimens with varying angles at temperatures spanning from 298 K to 873 K. As the angle of the specimens increased, the stress state at the centre of the specimens underwent a transition from pure shear to a mixed tensile-shear state, and subsequently to pure tensile. The stress triaxiality and equivalent plastic strain at the fracture position of the sheet in the state of stress triaxiality 0-0.3 were obtained.
2. Secondly, tests and simulations were conducted at temperatures ranging from 298 K to 873 K on uniaxial tensile and Nakazima specimens of varying widths. The stress state at the fracture location of the specimens exhibited a transition from single to double tension as the width of the specimens increased. The stress triaxiality and equivalent plastic strain at the fracture location of the sheet at a stress triaxiality of 0.3-0.666 were obtained.
3. The stress triaxiality and equivalent plastic strain at the fracture location were obtained by simulations. These data were then summarised to fit B-W curves at different temperatures. Subsequently, the temperature was introduced into the B-W criterion, resulting in the establishment of a unified expression for the B-W criterion at temperatures between 298 K and 873 K. The accuracy of the criterion was verified through the use of a tensile bending test.
4. As temperature increases, the B-W curve shifts upward, indicating that warm forming can effectively increase material elongation and improve moulding properties. In the actual production of auto parts, the fracture of parts can be reduced first by increasing the temperature. Secondly, the VUMAT subroutine containing B-W is invoked in ABAQUS before stamping to simulate the forming process to predict and avoid defects in the forming process. This has practical significance in terms of reducing the time required for mould design and improving the process solution, thereby reducing the cost of product development.

Acknowledgement

Thanks are given to RONGCHENG COMPAKS NEW ENERGY AUTOMOBILE CO, LTD, for supporting the joint development project.

REFERENCES

[1] Zu SJ, MAO Bo, HU Guangkui. Microstructure control and strengthening mechanism of high strength cold rolled dual phase steels for automobile applications. *Journal of Metals*, **2022**,58(04):551-566.

[2] Topilla L, Toros S. Analysis of the Fracture Behaviour of Dual-phase Steels Using the GISSMO and Johnson Cook Models. Transactions of FAMENA, **2023**, 47(3):79-95. https://doi.org/10.21278/TOF.473040522

[3] Liu Lixi, Zhu Jian, Li Zhiqiang. Fracture failure analysis of 6061 and 7075 aluminum alloys based on stress triaxiality and load parameters. *Journal of Experimental Mechanics*, **2017**, 32(03):342-350.

[4] Bao Y, Wierzbicki T. On fracture locus in the equivalent strain and stress triaxiality space. *International Journal of Mechanical Sciences*, **2004**, 46(1): 81-98. https://doi.org/10.1016/j.ijmecsci.2004.02.006

[5] GUI Liangjin, GAO Fuhai, FAN Zijie. Study of failure criterion of advanced high strength steel. *Journal of Solid Mechanics*, **2012**, 33(04):395-403.

[6] Yu Simiao, CAI Lixun, Yao Di, et al. Study on critical fracture criteria of metal materials under quasi-static conditions. *Chinese Journal of Mechanical Mechanics*, **2018**, 50(05):1063-1080.

[7] YU Wanqian, YU Rui, CUI Shitang. On ductile fracture of 30CrMnSiNi2A steel considering effects of stress triaxiality. *Explosion and Shock*, **2021**, 41(03):47-54.

[8] LI Ying, WU Weiguo, ZHU Haiqing et al. Fracture Properties of Ship-Build Mild Steel in Wide Range of Stress Triaxiality. *China Shipbuilding*, **2016**, 57(03):54-64.

[9] GUO Zitao, SHU Kaiou,GAO Bin, et al. J-C model based failure criterion and verification of Q235 steel. *Explosion and Shock*, **2018**, 38(06):1325-1332.

[10] CHEN Gang, XU Weifang, HE Peng, et al. Fracture failure characteristics of TC4 titanium alloy under different stress triaxiality, temperature and strain rate//Explosive Mechanics Committee of Chinese Mechanics Society, Key Laboratory of Shock Wave Physics and Explosive Physics, Institute of Fluid Physics, Chinese Academy of Physics. Proceedings of the Eighth National Conference on Explosive Mechanics. Institute of General Engineering, China Academy of Engineering Physics, **2007**:4.

[11] FU Qiutao. The Study on Failure Stress Type Criterion of Advanced High Strength Dual-Phase Steel Sheet Forming. *Shandong University of Technology*, **2022**.

[12] Zhao Gangyao, Yang Shengjin, Zhang Ranyang, et al. Research on the influence of stress triaxiality on fracture strain of 7075 as-cast aluminum alloy. *Journal of Plasticity Engineering*, **2018**, 25(01):192-198.

[13] Visagan A, Ganesh P, Ethiraj N, et al. Multi-objective optimization of single point incremental forming of 316L stainless steel using grey relational and principal component analsyes. Transactions of FAMENA, **2024**, 48(2): 85-99. https://doi.org/10.21278/TOF.482054923

[14] GB/T4338-2006; Metallic Materials High Temperature Tensile Test Method. China: General Administration of Quality Supervision, Inspection and Quarantine of the People's Republic of China, Standardization Administration of China: Beijing, China, **2006**.

[15] Li Y, Li D, Song H, et al. Temperature Dependency of Modified Mohr–Coulomb Criterion Parameters for Advanced High Strength Dual-Phase Steel DP780. *Metals*, **2024**, 14(6): 721. https://doi.org/10.3390/met14060721

[16] National Forging Standard Committee GB/T15825.8-2008 Sheet metal formability and test methods -- Part 8: Forming Limit diagram (FLD) test. Beijing: Standards Press of China, **2008**.

[17] Cui H, Li D, Fu Q, et al. Research on Forming Limit Stress Diagram of Advanced High Strength Dual-Phase Steel Sheets. Materials, **2023**, 16(13): 4543. https://doi.org/10.3390/ma16134543

[18] Bai Y, Wierzbicki T. A new model of metal plasticity and fracture with pressure and Lode dependence. International journal of plasticity, **2008**, 24(6): 1071-1096. https://doi.org/10.1016/j.ijplas.2007.09.004

[19] Bai Y, Wierzbicki T. Application of extended Mohr–Coulomb criterion to ductile fracture. International journal of fracture, **2010**, 161(1): 1-20. https://doi.org/10.1007/s10704-009-9422-8

[20] Bai Y, Wierzbicki T. A comparative study of three groups of ductile fracture loci in the 3D space. Engineering Fracture Mechanics, **2015**, 135: 147-167. https://doi.org/10.1016/j.engfracmech.2014.12.023

[21] Li Y, Luo M, Gerlach J, et al. Prediction of shear-induced fracture in sheet metal forming. *Journal of Materials Processing Technology*, **2010**, 210(14): 1858-1869. https://doi.org/10.1016/j.jmatprotec.2010.06.021

[22] Qi Shuang, CAI Lixun, Bao Chen, et al. Study on the stress triaxiality of ductile materials based on the full-range constitutive relationship. *Engineering Mechanics*, **2015**, 32(S1):27-32.

[23] Sima Aiping. Influence of stress triaxiality on material fracture. Shanghai Jiao Tong University, **2009**. (In Chinese)

[24] Khellafi H, Bendouba M, Meddah H M. Experimental and Numerical Analysis of Ductile Fracture of Polymeric Materials. Transactions of FAMENA, **2024**, 48(4):123-134. https://doi.org/10.21278/TOF.484062523

[25] Zhou Q, Establishment and application of fracture criterion for 304 stainless steel based on average stress triaxiality. Wuhan University of Technology, **2015**.

Submitted: 05.9.2024

Accepted: 19.02.2025

Yukuan Li
18763941690@163.com
Di Li*
Dongze Wu
18249877310@163.com
Yiqun Wang
w826433163@sina.cn
School of Transportation and Vehicle Engineering, Shandong University of Technology, Zibo 255000, China

Shaoxun Liu
lsx99ht@126.com
Rongcheng Compaks New Energy Automobile Co., Ltd, Rongcheng 264300, China

Tao Wang
19811729317@163.com
Xiaokun Wang
17753333424@163.com
School of Transportation and Vehicle Engineering, Shandong University of Technology, Zibo 255000, China

*Corresponding author:
hahali@sdut.edu.cn